



Using low-cost disposable immunosensor based on flexible PET screen-printed electrode modified with carbon black and gold nanoparticles for sensitive detection of SARS-CoV-2

Luís M.C. Ferreira^a, Isabela F. Reis^a, Paulo R. Martins^b, Luiz H. Marcolino-Junior^c, Marcio F. Bergamini^c, Jessica R. Camargo^d, Bruno C. Janegitz^d, Fernando C. Vicentini^{a,*}

^a Center of Nature Sciences, Federal University of São Carlos, Rod. Lauri Simões de Barros km 12, 18290-000, Buri, SP, Brazil

^b Institute of Chemistry, Federal University of Goiás, Av. Esperança, Goiânia, GO 74690-900, Brazil

^c Laboratory of Electrochemical Sensors (LabSensE) - Department of Chemistry, Federal University of Paraná, 81.531-980, Curitiba, PR, Brazil

^d Department of Nature Sciences, Mathematics and Education, Federal University of São Carlos, 13600-970, Araras, SP, Brazil

ARTICLE INFO

Keywords:

PET
Screen-printed electrode
Electrochemical immunosensor
Carbon black
Gold nanoparticles
Low-cost diagnosis
SARS-CoV-2

ABSTRACT

To help meet the global demand for reliable and inexpensive COVID-19 testing and environmental analysis of SARS-CoV-2, the present work reports the development and application of a highly efficient disposable electrochemical immunosensor for the detection of SARS-CoV-2 in clinical and environmental matrices. The sensor developed is composed of a screen-printed electrode (SPE) array which was constructed using conductive carbon ink printed on polyethylene terephthalate (PET) substrate made from disposable soft drink bottles. The recognition site (Spike S1 Antibody (anti-SP Ab)) was covalently immobilized on the working electrode surface, which was effectively modified with carbon black (CB) and gold nanoparticles (AuNPs). The immunosensing material was subjected to a multi-technique characterization analysis using X-ray diffraction (XRD), transmission electron microscopy (TEM), and scanning electron microscopy (SEM) with elemental analysis via energy dispersive spectroscopy (EDS). The electrochemical characterization of the electrode surface and analytical measurements were performed using cyclic voltammetry (CV) and square-wave voltammetry (SWV). The immunosensor was easily applied for the conduct of rapid diagnoses or accurate quantitative environmental analyses by setting the incubation period to 10 min or 120 min. Under optimized conditions, the biosensor presented limits of detection (LODs) of 101 fg mL⁻¹ and 46.2 fg mL⁻¹ for 10 min and 120 min incubation periods, respectively; in addition, the sensor was successfully applied for SARS-CoV-2 detection and quantification in clinical and environmental samples. Considering the costs of all the raw materials required for manufacturing 200 units of the AuNP-CB/PET-SPE immunosensor, the production cost per unit is 0.29 USD.

1. Introduction

Coronavirus disease 19 (COVID-19) has proven to be one of the greatest challenges for humanity in this century. Since the beginning of the outbreak in December 2019 in Wuhan, China, the pandemic has caused more than six million deaths around the globe [1,2]. Although a number of vaccines has already been developed, their distribution has primarily been concentrated in high and middle-income countries while low-income countries have remained largely neglected. Apart from that, the control of the spread of the disease still largely depends on social restrictions and mass testing; these measures are intended to help

prevent the increase in mortality associated with COVID-19 and the emergence of new potentially vaccine-resistant variants of the virus. The ongoing pandemic scenario requires testing solutions that are preferably inexpensive, portable, and reliable as part of a comprehensive approach in the fight against Covid-19 [3–5]. Apart from the problems related to the effective diagnosis of the COVID-19 disease, another major concern is environmental contamination since SARS-CoV-2 has proved to have a high survival rate on most biotic and abiotic surfaces over long periods of time. Thus, the risk of the virus spreading through indirect routes other than via direct contact with human-contaminated fluids should be considered – these indirect routes may particularly include

* Corresponding author.

E-mail address: fcvicentini@ufscar.br (F.C. Vicentini).

<https://doi.org/10.1016/j.talo.2023.100201>

Received 22 September 2022; Received in revised form 2 March 2023; Accepted 5 March 2023

Available online 10 March 2023

2666-8319/© 2023 The Authors. Published by Elsevier B.V. This is an open access article under the CC BY-NC-ND license (<http://creativecommons.org/licenses/by-nc-nd/4.0/>).

contaminated sewage, soil, or water [6,7].

Among the analytical strategies employed for the detection of SARS-CoV-2, RT-PCR (reverse transcription-polymerase chain reaction) is the most common approach. The RT-PCR detection technique involves high operational costs as it requires the use of highly-skilled analysts; in addition, the technique involves time-consuming procedures and the use of instrumentation that is less favorable to miniaturization. These factors make this technique unsuitable for application in remote and economically disadvantaged areas.

Another technique employed for the diagnosis of SARS-CoV-2 infection is via the conduct of serological tests. Unlike the RT-PCR technique, the serological technique does not involve RNA amplification; instead, the technique involves the detection of antibodies generated from an immune response to SARS-CoV-2. It is worth noting that although the serological technique is less expensive and provides an operationally faster diagnosis compared to the RT-PCR technique, it is not as accurate and consistent as the former, especially due to the window period of the immune response [8].

Analytical techniques that are based on the detection of viral proteins usually involve few steps and are perfectly consistent with the concepts of mass production and point-of-care (POC) analytical strategies, which are considered essentially important in both clinical and environmental analyses. Under these techniques, the detection is performed using colorimetric [9,10] or electrochemical methods. Electrochemical detection techniques are widely popular among researchers and analysts because the analytical response is not dependent on the sensor size and the required instrumentation can be easily miniaturized to produce portable devices without compromising relevant analytical features such as sensitivity [11–13]. Under the electrochemically-based analytical detection approach, one can employ different agents for the recognition of antigens. Some of the agents employed for the recognition of antigens include the angiotensin-converting enzyme-2 (ACE2), the functional host receptor which binds to the virus transmembrane spike (S) protein, which is the most aimed biomarker for SARS-CoV-2 detection [9,14,15]. Other recognition elements comprise synthetic peptides [16], molecularly imprinted polymers [17,18], or specific antibodies. These biological recognition agents can discriminate specific targets in the viral structure such as spike and nucleocapsid (N) proteins [19–22].

In an attempt to improve the performance and efficiency of electrochemical biosensors, nanostructured materials and biorecognition agents have been successfully incorporated into the architecture of the sensing electrodes [23]. The resulting nano-bio interfaces function as a suitable platform for the application of different biosensing approaches. In this context, carbon black (CB) has emerged as an incredibly cost-effective alternative among the wide range of nanomaterials. CB has been found to have outstanding properties; these include high surface area, excellent conductivity, and fast charge transfer kinetics [20, 24]. Significant improvements in detection can be achieved by conjugating CB with gold nanoparticles (AuNPs); the incorporation of AuNPs into the sensing platform provide an interesting conductive and biocompatible substrate for protein attachment via thiolated cross-linkers without loss of bioactivity [25]. The hybrid material which is composed of CB decorated with AuNPs can provide a suitable microenvironment for antibody immobilization, and this can effectively promote enhanced electrochemical response with high sensitivity and specificity [26,27].

This work reports the development and application of a label-free nanostructured immunosensor for the detection of SARS-CoV-2 spike protein (SP); the immunosensor was constructed using carbon ink-based PET electrode, modified with CB matrix conjugated with AuNPs, capable of anchoring anti-SP antibodies. The proposed sensing device was easy to construct and its modification process was simple and straightforward. The sensor was constructed using low-cost and highly abundant materials; this allows it to be produced in mass quantities. All these factors make the electroanalytical device highly versatile and suitable for application in POC assays with a view to performing rapid efficient

diagnoses of SARS-CoV-2 and precise environmental analyses.

2. Experimental

2.1. Reagents and solutions

The following reagents and chemicals employed in the experiments were acquired from Sigma-Aldrich: gold (III) chloride, Sodium borohydride, Glutaraldehyde (GA) solution 25% (v/v), trisodium citrate dihydrate, potassium ferricyanide, potassium ferrocyanide, potassium monohydrogen phosphate, potassium dihydrogen phosphate, potassium chloride, magnesium chloride, sodium dihydrogen phosphate, sulfuric acid, hydrochloric acid, sodium chloride, ammonia, calcium chloride, alanine, aspartic acid, cysteine, glutamic acid, glycine, histidine, isoleucine, leucine, lysine, methionine, phenylalanine, proline, serine, threonine, tryptophan, tyrosine, valine, ascorbic acid, albumin, urea, 1,4- α -D-Glucan-glucanohydrolase (α -amylase from human saliva), and human serum from male AB clotted whole blood (sterile-filtered). Cystamine dihydrochloride (Cys) and Bovine serum albumin (BSA) (99%) were purchased from Nfinitu Tech LLC (USA). Carbon black (CB) powder (VCX72R) was obtained from Cabot®(USA). SARS-CoV-2 Spike S1-His-Recombinant Protein (SP, 76.45 kDa) and SARS-CoV-2 Spike S1 Antibody (anti-SP Ab) were acquired from Sino Biological (China). Graphite powder was acquired from Fischer Chemical (USA) while Silver Conductive Paint was obtained from EMS (USA). Colorless nail polish for nail care (Base Brilho Cuidados, Cora®, São Paulo, Brazil) was used as the polymer-based vehicle for conductive ink production. Polyethylene terephthalate (PET) sheets were acquired from discarded soft-drink bottles found in the local market in Campina do Monte Alegre (São Paulo, Brazil).

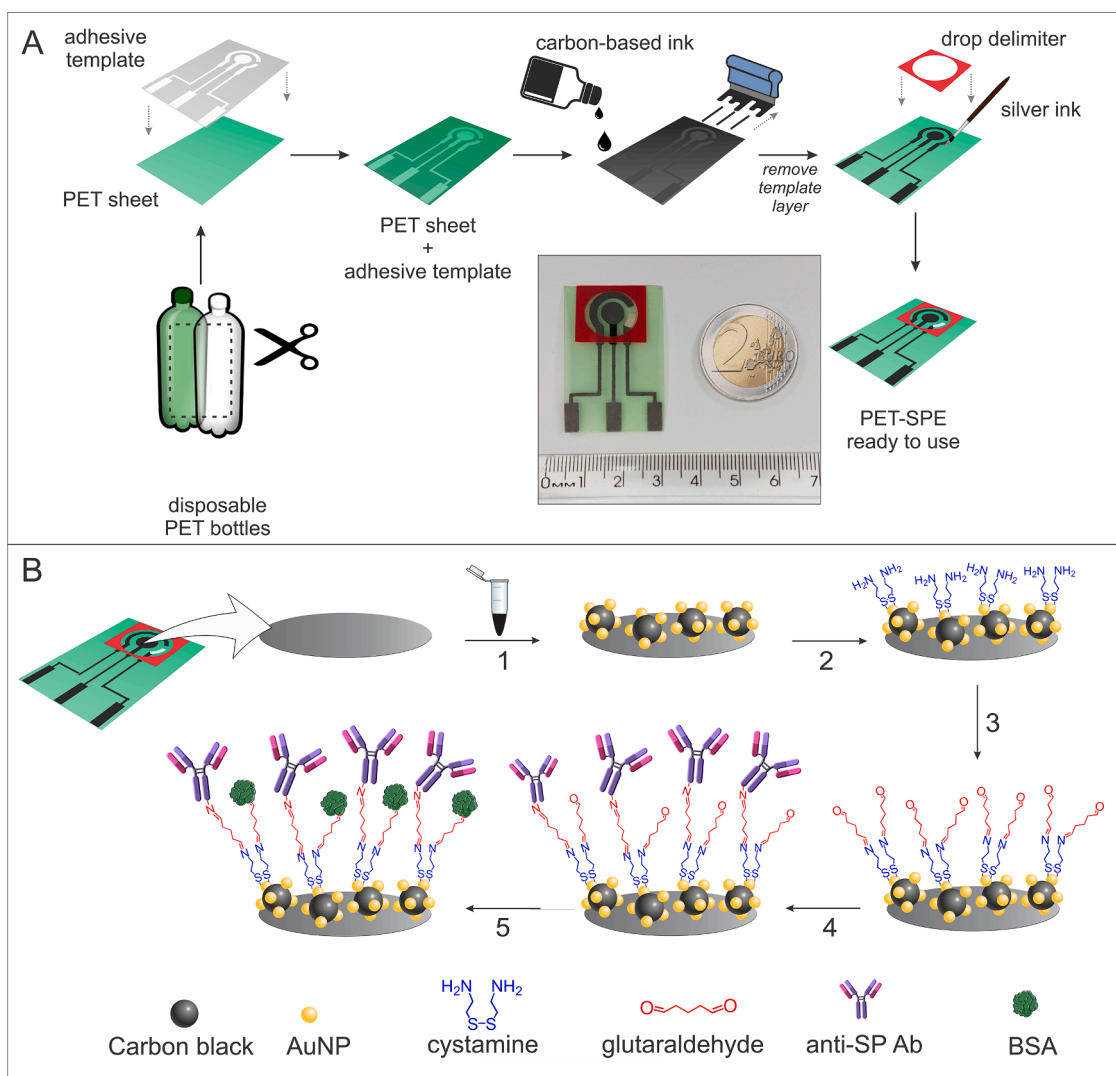
All solutions were prepared using ultrapure water (with resistivity $\geq 18 \text{ M}\Omega\cdot\text{cm}$) from a Milli-Q purification system (Millipore®).

2.2. Apparatus

All electrochemical measurements were performed using an AutolabPGSTAT101 potentiostat/galvanostat operated via the NOVA 2.1.4 software (Metrohm Autolab B.V, The Netherlands). A Jenway 3510 pH-meter was used to perform the pH measurements. The morphological characterization of the modified PET-SPE was performed using transmission electron microscopy (TEM, JEOL, JEM-2100) and scanning electron microscopy (SEM, JEOL model JSM 7100-F), while elemental analysis was conducted using energy dispersive spectroscopy (EDS). The generated images were analyzed using the ImageJ 1.53k software (Rasband, W.S., U. S. National Institutes of Health, Bethesda, Maryland, USA). X-ray diffraction (XRD) analysis was performed using a Bruker D8 Discover diffractometer under Cu-K α_1 radiation.

2.3. Synthesis of gold nanoparticles

The AuNPs dispersion was synthesized based on a technique reported in the literature, with some adaptations [28,29]. Initially, an amount of 758.4 mg of AuCl₃ was dissolved in 50.0 mL of 0.1 mol L⁻¹ HCl, and this gave rise to 0.05 mol L⁻¹ HAuCl₄ solution. Thereafter, an amount of 590 μL of this solution was added to 90 mL of water under continuous vigorous stirring at room temperature, giving the solution a pale-yellow color. After 1 min of stirring, 1.0 mL of 38.8 mmol L⁻¹ sodium citrate was added to the mixture which was kept under stirring again for one more minute. Finally, a solution composed of 1.0 mL of 0.075% sodium borohydride and 38.8 mmol L⁻¹ sodium citrate was added to the mixture as a reducing agent, and this instantly changed the dispersion color to ruby red. The mixture was then kept under stirring for 10 min. The pH of the resulting colloidal solution was adjusted to 6.0 using 1.0 mol L⁻¹ KOH to avoid the destabilization of particles due to citrate protonation. Finally, the AuNP dispersion was transferred to a dark flask and stored at 4 °C.



Scheme 1. Schematic representation of (A) the steps involving the fabrication of the flexible PET-SPE. Inset: Picture of real PET-SPE; (B) preparation of the AuNP-CB/PET-SPE immunosensor used for the detection of SARS-CoV-2 SP: 1) drop casting of AuNP-CB dispersion; addition and incubation of 2) 10 mmol L⁻¹ cystamine, 3) 2.5% glutaraldehyde, 4) 1.0 μg mL⁻¹ anti-SP ab, 5) 1% BSA (for blocking non-binding sites).

2.4. Fabrication of carbon ink-based flexible PET-SPE and preparation of AuNP-CB/PET-SPE immunosensor

Scheme 1A shows the process involving the fabrication of the PET-SPE. The conductive ink was prepared based on a procedure previously reported in the literature [30,31]; under this procedure, an amount of 18.9 g of graphite powder was added to 27 g of nail polish, which resulted in a final suspension with ~ 41% (m/m) carbon content. This suspension was subjected to 3 cycles of centrifugation at 3500 rpm for 3 min in a dual asymmetric centrifuge SpeedMixer™ Dac 150.1 FVZ-K (FlackTec Inc). For the construction of the electrode substrate, polyethylene terephthalate (PET) sheets acquired from discarded soft-drink bottles were prepared by washing, sanding and cutting, and this yielded a 25 × 35 mm PET piece. An adhesive paper sheet finely cut based on the sensor template (via cutting printer Silhouette, Cameo 3) was applied to delimit the electrode area over the PET sheet. After that, the graphite ink was applied on the sheet set using a spatula. Subsequently, the adhesive template was removed and discarded before the total drying of the ink. The resulting device consisted of a centered working electrode ($\varnothing = 5.0$ mm), a surrounding counter electrode, and a pseudo-reference electrode, which was manually covered with silver ink using a fine tip brush. A round adhesive plastic layer was added to

delimitate the drop area, with a cell volume of 100 μL.

To obtain the AuNP-CB/PET-SPE immunosensor, the electrode was subjected to five modification procedures; these procedures are summarized in Scheme 1B. First, 0.5 mg of CB powder was added to 500 μL of AuNP colloidal solution, and this yielded AuNP-1.0 mg mL⁻¹ CB dispersion. After that, an amount of 10 μL of this dispersion was cast onto the working SPE surface and dried in vacuum chamber for 30 min. Prior to performing any further modification, the AuNP-CB/PET-SPE surface was subjected to electrochemical pre-treatment in order to activate it. The electrochemical pre-treatment was performed using 10 successive voltammetric cycles in the potential range of -0.5 V to 1.2 V at 0.1 Vs⁻¹ using 0.1 mol L⁻¹ H₂SO₄. Secondly, an amount of 25 μL of 10 mmol L⁻¹ cystamine (Cys) dihydrochloride solution was placed over the working electrode area and left to incubate for 1 hour at room temperature. The third modification procedure involved the addition of 25 μL of 2.5% (m/v) glutaraldehyde (GA) solution on the working electrode area for 1 hour. The fourth procedure involved the incubation of the SPE surface with 25 μL of 1.0 μg mL⁻¹ Anti-SP Ab in 0.1 mol L⁻¹ phosphate buffered-saline (PBS), pH 7.4, for 2 h. In the final modification procedure (5), an amount of 25 μL of 1% (m/v) BSA was used to block non-specific binding sites on the electrode surface for 30 min. At the end of each of the procedures mentioned above, the electrode was

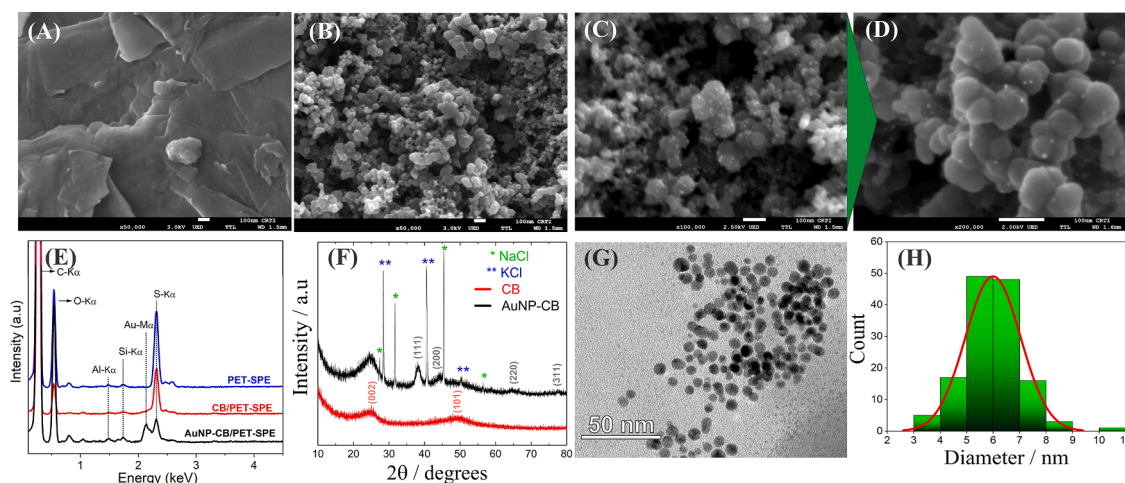


Fig. 1. SEM images obtained for PET-SPE (A), CB/PET-SPE (B) and AuNP-CB/PET-SPE (C and D), and their respective EDS spectra (E); XRD pattern of CB and AuNPs-CB (F); TEM images of gold nanoparticles (G) and the histogram of the particle size distribution (H).

washed with 0.1 mol L⁻¹ PBS (at pH 7.4). Detailed information on the total costs incurred in the production of 200 units of the AuNP-CB/PET-SPE immunosensor can be found in Table S1.

2.5. Preparation of samples

River water samples were obtained from the Paranapanema River in Campina do Monte Alegre (São Paulo, Brazil). Artificial saliva was produced based on two procedures reported in the literature, with few modifications [32]; the procedures involved dissolving the following substances to their respective concentrations in 100.0 mL of deionized water: 15.6 mmol L⁻¹ potassium chloride, 2.6 mmol L⁻¹ potassium dihydrogen phosphate, 0.2 mmol L⁻¹ magnesium chloride, 2.6 mmol L⁻¹ sodium dihydrogen phosphate, 10 mmol L⁻¹ sodium chloride, 4.4 mmol L⁻¹ ammonia, 1.4 mmol L⁻¹ calcium chloride, 0.0371 mmol L⁻¹ alanine, 0.012 mmol L⁻¹ aspartic acid, 0.05 mmol L⁻¹ cysteine, 0.0265 mmol L⁻¹ glutamic acid, 0.1185 mmol L⁻¹ glycine, 0.0064 mmol L⁻¹ histidine, 0.0221 mmol L⁻¹ isoleucine, 0.0221 mmol L⁻¹ leucine, 0.0185 mmol L⁻¹ lysine, 0.0002 mmol L⁻¹ methionine, 0.0176 mmol L⁻¹ phenylalanine, 0.0017 mmol L⁻¹ proline, 0.02 mmol L⁻¹ serine, 0.0243 mmol L⁻¹ threonine, 0.01 mmol L⁻¹ tryptophan, 0.0116 mmol L⁻¹ tyrosine, 0.0154 mmol L⁻¹ valine, 0.005 mmol L⁻¹ ascorbic acid, 0.0004 mmol L⁻¹ albumin, 2.9 mmol L⁻¹ urea, and 200 U mL⁻¹ α -amylase.

To reproduce a clinical assay condition and evaluate the matrix interactions, the control samples (negative samples) of human serum, artificial saliva, and river water were prepared using 1:1000 dilution in PBS solution (pH 7.4). For the fortified samples (positive), an aliquot SP solution was added to the sample before dissolution in the buffer solution; this yielded a final SP concentration of 76.5 pg mL⁻¹. After the dilution process, an amount of 50 μ L of each sample was added to the working electrode surface and subjected to static incubation for different periods of time (10 min or 120 min).

2.6. Electrochemical and analytical evaluation of the AuNP-CB/PET-SPE immunosensor

The electrochemical characterizations of the PET-SPE, CB/PET-SPE, and AuNP-CB/PET-SPE were performed using cyclic voltammetry in two different conditions: i) in 0.1 mol L⁻¹ H₂SO₄; ii) in 0.1 mol L⁻¹ KCl in the presence of 2.0 mmol L⁻¹ [Fe(CN)₆]^{4-/3-} used as electrochemical probe to estimate the respective active areas of the electrodes and the heterogeneous electron transfer rate constant values, k^0 (see Supporting Information). Cyclic voltammetry analysis was performed using 4.0 mmol L⁻¹ [Fe(CN)₆]^{4-/3-} and 0.1 mol L⁻¹ PBS (pH 7.4) in order to evaluate the effect of further modifications in the electrodes in terms of

the molecular attachment of anti-SP Ab. For analytical purposes, the AuNP-CB/PET-SPE immunosensor was evaluated by square-wave voltammetry (SWV) using 4.0 mmol L⁻¹ [Fe(CN)₆]^{4-/3-} in 0.1 mol L⁻¹ PBS (pH 7.4) before and after the incubation step in the presence of the target analyte. The normalized SWV current variation, $(I_0 - I)/I_0$, was used to minimize any variations in electrode area potentially caused by the SPE manual manufacturing process.

The limit of detection (LOD) of the AuNP-CB/PET-SPE immunosensor was estimated using five-parameter logistic regression (SPL) and Eqs. (1)–3 in the entire concentration range. This approach is useful for biological assays and situations where the signal intensity shows a logarithm dependence on the analyte concentration [2,33].

$$L_C = \mu_{\text{blank}} + t_{(95\%, n-1)} \times \sigma_{\text{blank}} \quad (1)$$

Here, L_C is the limit of the blank – this is a critical value related to blank signal intensities which has 5% probability of resulting in a false positive; μ_{blank} is the mean of signal intensities for $n = 9$ blank replicates; σ_{blank} is the standard deviation (SD) of the blank replicates; and $t_{(95\%, n-1)}$ is the value of t-Student for $n - 1$ degrees of freedom with 95% of confidence.

$$L_D = L_C + t_{(95\%, m(n-1))} \times \sigma_{\text{test}} \quad (2)$$

In Eq. (2), L_D stands for the limit of detection in the signal domain – i. e., the lowest signal value with 5% probability of generating a false negative result; σ_{test} is the pooled standard deviation of $(I_0 - I)/I_0$ values for $n = 3$ replicates for each point of $m = 10$ concentrations of the curve, which can be calculated using Equation 3; and $t_{(95\%, m(n-1))}$ is the value of t-Student for $m(n - 1)$ degrees of freedom with 95% of confidence.

$$\sigma_{\text{test}} = \sqrt{\frac{\sum_{i=1}^m \sigma_i^2}{m}} \quad (3)$$

3. Results and discussion

3.1. Morphological characterization of the electrode materials

The SEM images of the PET-SPE (Fig. 1A) show the conductive carbon ink with low roughness pattern. The modification of the electrode with CB dispersion led to an increase in the roughness of the surface; the surface was characterized by the presence of CB nanoparticles of different sizes, with most of them varying between 20 nm and 100 nm (Fig. 1B), and their relative homogenous distribution across the analyzed area. The respective EDS spectrum (in blue, Fig. 1E) shows a

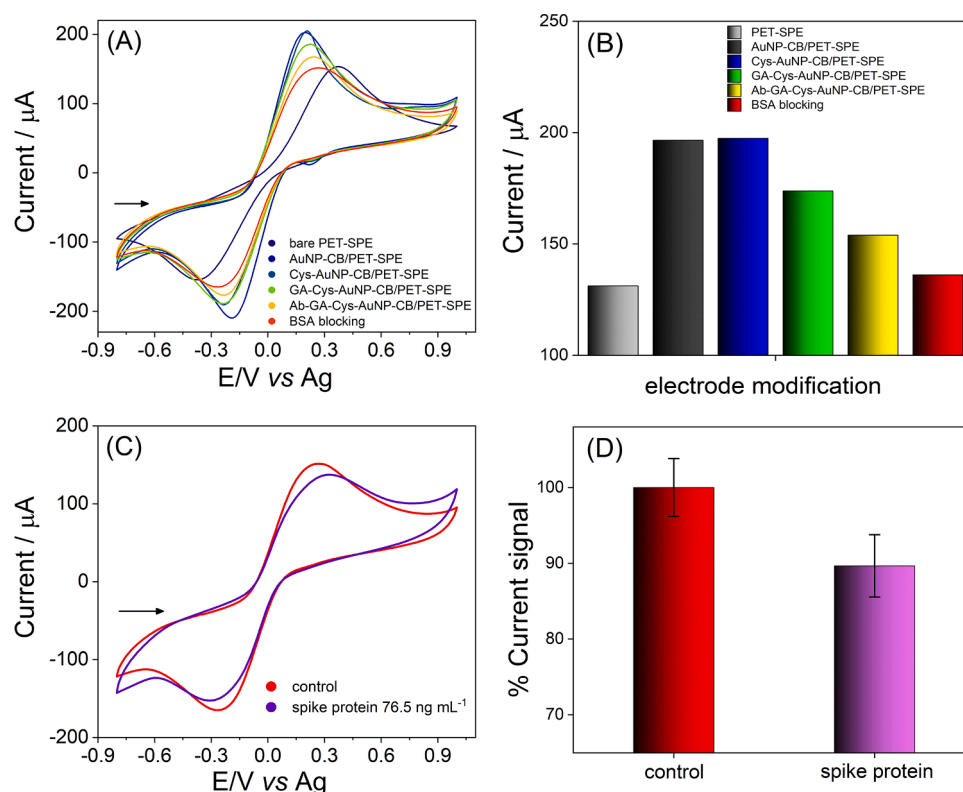


Fig. 2. (A) CV response recorded after each of the steps taken to modify PET-SPE. (B) Comparative column graph of oxidation current for each electrode modification procedure; (C) spike protein detection CV response by antigen capture by immobilized antibody; and (D) respective column graph of relative current response. All measurements were conducted using $4.0 \text{ mmol L}^{-1} [\text{Fe}(\text{CN})_6]^{4-/-3-}$ in 0.1 mol L^{-1} PBS (pH 7.4) with potential range from -0.8 to 1.0 V , and at scan rate of 50 mVs^{-1} .

typical carbon-based material energy dispersion profile. The intense sulfur peak (2.31 keV) and the silicon (1.73 keV) and aluminum (1.48 keV) peaks observed in the profile are related to the polish nail components present in the conductive ink [30]. The incorporation of AuNPs in the system produced a nanostructured film with well-dispersed nanoparticles along with the CB matrix, exhibiting a lighter contrast due to the weight-dependent electron scattering (Fig. 1C and D). The respective EDS spectrum shows the characteristic peak assigned to Au-M α transition in 2.12 keV. A more detailed view of the AuNPs dispersion can be found in Fig. 1G; this figure was used to generate the histogram of the particle size distribution (Fig. 1H), with the particles diameter varying between 3 and 11 nm and mean of $(6 \pm 1) \text{ nm}$.

The results obtained from the XDR analysis of CB (Fig. 1F) showed the carbon material characterized by the presence of a wide peak at 24.5° and a weak peak at 48.6° corresponding to graphite planes (002) and (101), respectively, which is in line with the data from the Joint Committee on Powder Diffraction Standards (JCPDS 75-1621). The upper spectrum in black corresponds to the AuNP-CB dried dispersion; this spectrum exhibits four distinct peaks with the diffraction angles of 38.0° , 44.0° , 64.5° , and 77.3° indexed as the crystal planes (111), (200), (220), and (311) corresponding to AuNPs (JCPDS 04-0784). The remaining sets of peaks (27.5° , 31.7° , 45.4° , 56.4°) and (28.5° , 40.5° , 50.3°) exhibited a high crystalline pattern, and were respectively assigned to NaCl (JCPDS 05-0628) and KCl (41-1476), which are remnants of the synthesis of AuNPs.

3.2. Electrochemical characterization of the AuNP-CB/PET-SPE

Figure S1 presents a comparative analysis of the cyclic voltammograms obtained for the PET-SPE, CB/PET-SPE, and AuNP-CB/PET-SPE applied in $0.1 \text{ mol L}^{-1} \text{ H}_2\text{SO}_4$. The addition of the AuNP-CB dispersion on the electrode surface resulted in a typical voltammetric response for polycrystalline gold, which is characterized by three anodic peak

currents at around 0.456 V, 0.780 V and 1.000 V and assigned to specific voltammetric signatures of different index crystal planes of gold – this is a reflection of the oxidation of AuNPs to oxide species. A well-defined cathodic peak is observed at 0.270 V, while other less intense peaks are observed at 0.750 V and 0.050 V, which are related to the subsequent reduction of the oxide species back to metallic gold [34–36].

The electroactive areas of the PET-SPE, CB/PET-SPE, AuNPs/PET-SPE, and AuNPs-CB/PET-SPE were estimated by cyclic voltammetry using $2.0 \text{ mmol L}^{-1} [\text{Fe}(\text{CN})_6]^{3-}$ and $0.10 \text{ mol L}^{-1} \text{ KCl}$ solution (see Fig. S2), based on the Randles-Sevcik equation. The electroactive areas obtained for the PET-SPE, CB/PET-SPE, AuNPs/PET-SPE, and AuNP-CB/PET-SPE were 0.102 cm^2 , 0.130 cm^2 , 0.152 cm^2 , and 0.207 cm^2 , respectively; these result show that the modification of the electrodes with nanomaterials significantly altered the morphology of the electrodes, increasing their surface roughness. The corresponding changes in the charge transfer kinetics were evaluated using the apparent heterogeneous electron transfer rate constant, k^0 ; this was estimated based on the Nicholson's method for quasi-reversible systems [37]. The k^0 values were derived from the angular coefficients of the resulting curves: $3.3 \times 10^{-4} \text{ cm s}^{-1}$ for PET-SPE, $4.2 \times 10^{-4} \text{ cm s}^{-1}$ for CB/PET-SPE, $5.53 \times 10^{-4} \text{ cm s}^{-1}$ for AuNPs/PET-SPE, and $7.8 \times 10^{-4} \text{ cm s}^{-1}$ for AuNPs-CB/PET-SPE. The results obtained point to an increase in reversibility as the nanomaterials are incorporated onto the PET-SPE surface.

Fig. 2A shows the cyclic voltammograms recorded after each of the steps taken to modify the PET-SPE surface in order to produce an efficient immunosensing response to SARS-CoV-2 SP. The first modification procedure, which involved the incorporation of AuNP-CB dispersion onto the PET-SPE surface, caused a significant increase in the current response of the redox probe and a noticeable improvement in reversibility, as previously discussed, with a substantial decrease of ΔE value from 0.745 V in PET-SPE (gray line) to 0.365 V in AuNP-CB/SPE (blue line). This enhanced quasi-reversible system has the required

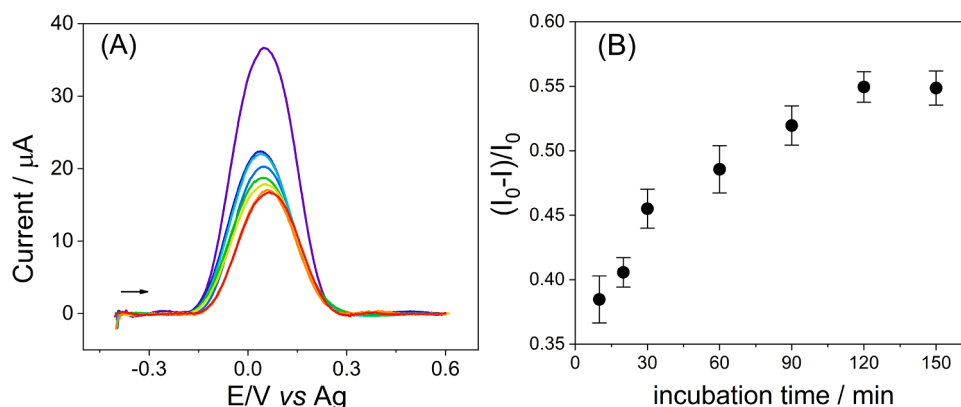


Fig. 3. (A) SWV responses obtained in different incubation periods based on the application of 7.65 ng mL^{-1} SP in the presence of $4.0 \text{ mmol L}^{-1} [\text{Fe}(\text{CN})_6]^{4-/3-}$ in 0.1 mol L^{-1} PBS (pH 7.4), in the time range of 10 - 120 min. SWV conditions: $f = 5 \text{ Hz}$; $a = 100 \text{ mV}$; $\Delta E = 2 \text{ mV}$. (B) Normalized current variation, $(I_0 - I)/I_0$, vs incubation time.

characteristics considered suitable for the biosensing application. The blue voltammogram indicates the response related to the binding of Cys to AuNPs surface which happens through the disulfide groups. At this point, the slight improvement observed in the anodic current is attributed to the favorable electrostatic interactions between the NH_3^+ groups of Cys and the negatively charged redox probe. The successive decreases observed in the current response point to a decline in charge transfer kinetics which is associated with the molecular binding of the modifying materials: GA via condensation reaction with Cys (green line); Anti-SP binding to GA free sites (yellow line); and BSA blocking of non-specific binding sites (red line). At this point, the modification process is fulfilled, and the antigen detection is performed by incubation of the modified surface for 30 min incubation in 76.5 ng mL^{-1} spike protein solution in PBS buffer, resulting in the voltammogram of Fig. 2C, where the 10.4% current decrease from the control record verify the antigen capturing by the immobilized antibody.

3.3. Analytical response of the AuNP-CB/PET-SPE immunosensor to SARS-CoV-2 spike protein

The analytical response of the Au-CB/PET-SPE immunosensor was evaluated using SWV; the application of this voltammetric technique allows the detection of small perturbations in the redox system related to surface interactions. The SWV experiments were performed in the presence of a mixture containing 4.0 mmol L^{-1} of both $[\text{Fe}(\text{CN})_6]^{4-}$ and $[\text{Fe}(\text{CN})_6]^{3-}$ in 0.1 mol L^{-1} PBS (pH 7.4) in the potential range of -0.4 to 0.6 V , under the following optimized conditions: frequency (f) = 5 Hz ; pulse amplitude (a) = 100 mV ; and potential increment (ΔE) = 2 mV . The SW voltammograms were recorded after different incubation periods, ranging between 10 and 120 min, in the presence of the target analyte. The voltammograms obtained along with the time-dependent normalized current response of the sensor are shown in Fig. 2. The results obtained point to a decrease in peak current as the incubation period increases in the presence of 7.65 ng mL^{-1} SP solution; this behavior is attributed to the interaction affinity between the SP and anti-SP Ab immobilized on the AuNP-CB/PET-SPE, which caused a more effective blockade of the surface when long loading periods were employed.

For the incubation period of 120 min and beyond, the sensor exhibits higher yet stabilized current loss with mean value of approximately 55%; this is considered to be the optimal interval at which the highest sensitivity condition can be achieved. The result obtained for this incubation period shows that it is not suitable for rapid diagnostic test. Surprisingly, a calibration curve recorded using 10 min incubation showed mean current suppression/loss of 38%. Based on these results, two calibrations set conditions were evaluated: i) an optimized

condition using 120 min incubation of SP solutions in order to obtain a more sensitive and precise response for quantitative analyses; and ii) a calibration based on 10 min SP incubation targeted at obtaining qualitative response applied as a rapid diagnostic test for SARS-CoV-2.

Figs. 3A and 3B present the square-wave voltammograms obtained from the increase in SP concentrations from 7.65×10^{-15} to $7.65 \times 10^{-6} \text{ g mL}^{-1}$ for 10 min and 120 min, respectively. Under both conditions, the calibration plots exhibited linear relationships Eqs. (4) and (5) between Ip and logarithm of SP concentration range from 7.65×10^{-14} to $7.65 \times 10^{-8} \text{ g mL}^{-1}$ (Fig. 3D).

$$(I_0 - I)/I_{0[10 \text{ min}]} = (0.456 \pm 0.007) + (0.037 \pm 0.006) \times \log C_{\text{SP}} = 0.989 \quad (4)$$

$$(I_0 - I)/I_{0[120 \text{ min}]} = (0.781 \pm 0.009) + (0.099 \pm 0.002) \times \log C_{\text{SP}} = 0.999 \quad (5)$$

As can be noted, the degree of sensitivity obtained from the application of 120 min incubation is found to be 2.7-fold higher compared to that obtained for the incubation time of 10 min; this can significantly affect the detectability accuracy of the sensor. The limit of detection (LOD) of the AuNP-CB/PET-SPE was estimated based on five-parameter logistic regression (5PL) fitted curves presented in Figure S3. The LOD values obtained for the application of 10 min and 120 min incubation periods were 101 fg mL^{-1} and 46.2 fg mL^{-1} , respectively. The limit of quantification (LOQ = $3.33 \times \text{LOD}$) was estimated for the 120 min incubation time only; the LOQ value obtained was 154 fg mL^{-1} .

A thorough analysis was conducted in order to evaluate the performance/efficiency of the AuNP-CB/PET-SPE immunosensor in detecting SARS-CoV-2 spike protein in three different samples: i) river water (environmental sample); ii) artificial saliva and iii) blood serum (clinical samples). All the samples were spiked with 76.5 pg mL^{-1} of the target protein and subjected to 10 min and 120 min incubation periods; the samples were analyzed based on the respective calibration with a view to obtaining qualitative and quantitative operational modes of the sensor. Fig. 4 presents the square-wave voltammograms obtained for the tested samples. The results obtained for the negative samples (in the absence of antigen) under the 10 min and 120 min incubation periods did not show any significant differences. The $(I_0 - I)/I_0$ magnitudes and error bars shown in Fig. 4D are based on the mean values and grouped data standard deviation, respectively. Fig. 5

The negative samples presented a low current decrease, which was less than 6.7% of the loss from the blank signal; the value recorded was less than the value required to obtain the LOD values in the two calibration conditions. This result pointed to the low interference of the matrices of the samples. As expected, compared to the positive samples under the 10 min incubation regime, the positive samples under the 120

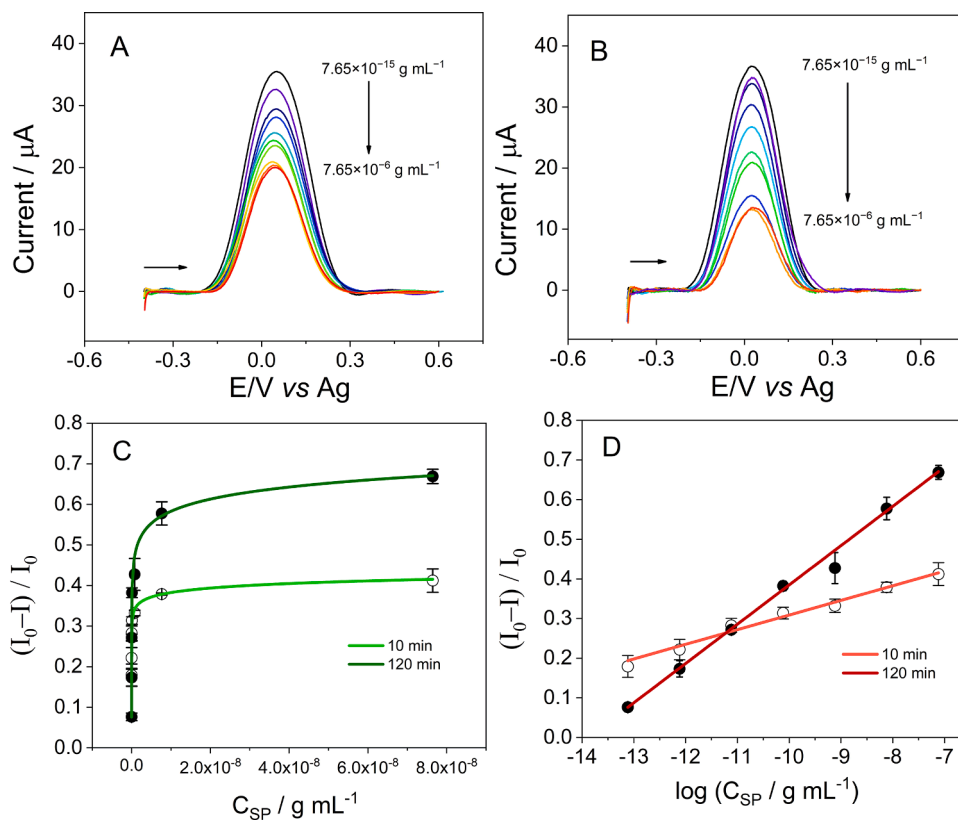


Fig. 4. SWV response obtained from an increase in SP concentrations (from 7.65×10^{-15} to $7.65 \times 10^{-6} \text{ g mL}^{-1}$) in the presence of 0.1 mol L^{-1} PBS (pH 7.4) containing $4.0 \text{ mmol L}^{-1} [\text{Fe}(\text{CN})_6]^{4-/-3-}$ after (A) 10 min, and (B) 120 min of incubation; (C) Current response vs. SP concentration plot; (D) linear calibration plot using $\log C_{\text{SP}}$. SWV conditions: $f = 5 \text{ Hz}$; $a = 100 \text{ mV}$; $\Delta E = 2 \text{ mV}$.

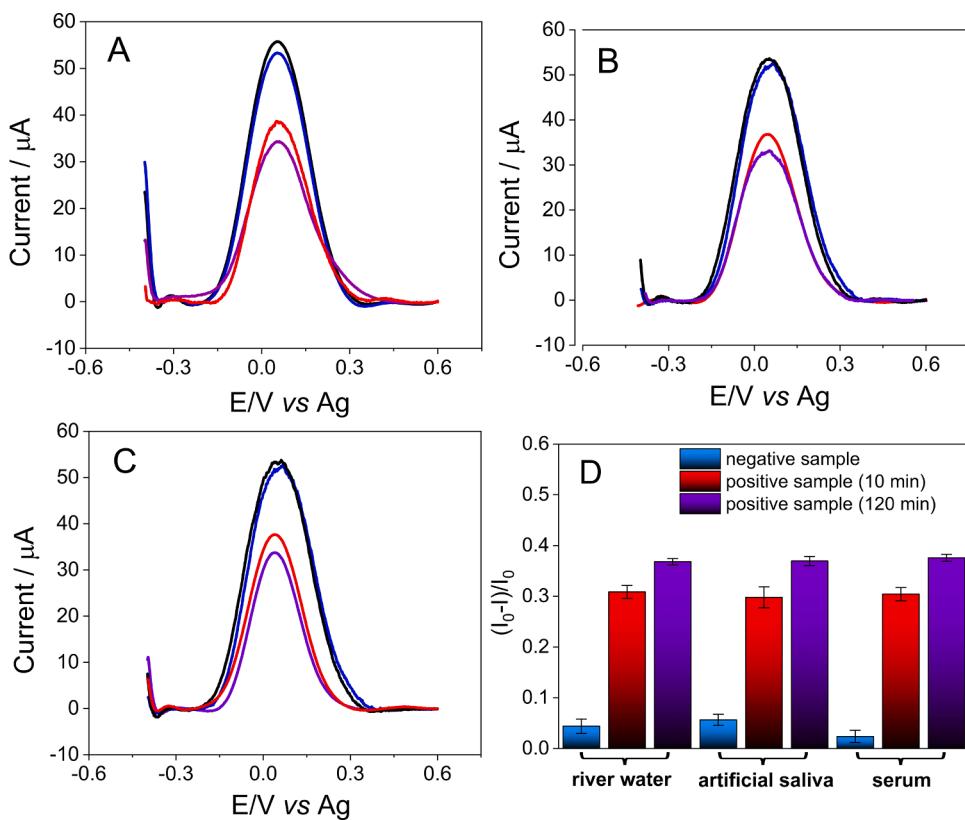


Fig. 5. SWV responses obtained for the AuNP-CB/PET-SPE immunosensor applied in 0.1 mol L^{-1} PBS pH (7.4) containing $4.0 \text{ mmol L}^{-1} [\text{Fe}(\text{CN})_6]^{4-/-3-}$ after the incubation of the samples: (A) river water, (B) artificial saliva, and (C) blood serum. (D) Comparative normalized current variation response. Color patterns represent blank solution (black line), negative sample (blue), and positive sample containing 76.5 pg mL^{-1} SP in 10 min incubation (red) and 120 min incubation (violet). SWV conditions: $f = 5 \text{ Hz}$; $a = 100 \text{ mV}$; $\Delta E = 2 \text{ mV}$.

Table 1

Comparative analysis of the results obtained for the positive samples evaluated under the two incubation regimes based on the application of the AuNP-CB/PET-SPE immunosensor.

Sample	river water	artificial saliva	blood serum
Added SP concentration / pg mL^{-1}	76.5	76.5	76.5
10 min incubation (qualitative assay)	+	+	+
120 min incubation (quantitative assay) / pg mL^{-1}	(68 \pm 9)	(71 \pm 13)	(81 \pm 14)

Table 2

Comparative analysis of low-cost SARS-CoV-2 tests reported in the literature based on spike protein detection.

Detection	Biorecognition	sample	time required	LOD	Cost/unit USD	Ref.
SWV ¹	antigen-antibody affinity	saliva/serum	10 min	101 fg mL^{-1}	0.29	this work
SWV ¹	antigen-ACE2 ² affinity	oro/nasopharyngeal fluid/saliva	6.5 min	229 fg mL^{-1}	1.50	[14]
EIS ³	antigen-antibody affinity	spike protein solution in PBS	~10 min	1.065 fg mL^{-1}	5	[38]
EIS ³	antigen-antibody affinity	serum	~90 min	0.5 $\mu\text{g mL}^{-1}$	10.11 ⁴	[39]
EIS ³	antigen-ACE2 ² affinity	oro/nasopharyngeal fluid/saliva	4 min	2.18 fg mL^{-1}	4.67	[40]
EIS ³	antigen-aptamer affinity	nasopharyngeal fluid	15 min	not informed	0.31 ⁵	[41]
amperometric ⁶	antigen-invertase conjugated aptamer affinity	saliva	60 min	5.27 pmol L^{-1} (0.4 ng mL^{-1})	3.2	[42]
Colorimetric	antigen-ACE2 ² affinity	oro/nasopharyngeal fluid	5 min	0.154 pg mL^{-1}	0.15	[9]
Chemiluminescent lateral flow	antigen-antibody affinity	spike protein solution in PBS	16 min	0.1 ng mL^{-1}	0.9	[43]

¹ SWV: Square-wave voltammetry;

² ACE2: Angiotensin-converting enzyme-2;

³ EIS: Electrochemical impedance spectroscopy;

⁴ converted from euro (€);

⁵ converted from pound sterling (£);

⁶ Indirect current response based on glucose measurement (in mg/dL) of Accu-Chek GuideMe glucometer.

min incubation regime exhibited a higher current loss and lower standard deviation values considering the measurements performed in triplicate - this can be attributed to the affinity equilibrium state observed at longer periods of incubation. The results obtained for the positive samples are shown in Table 1.

Although a huge number of works reported in the literature have frequently pointed out that their sensing devices are of low cost, few of these works have actually presented the specific cost per test unit. For comparison purposes, Table 2 presents an outline of the data collected on different low-cost analytical devices reported in the literature which have been used for SARS-CoV-2 tests based on spike protein detection. As can be observed, our test reported in the present study stands out among the tests with the lowest cost per unit, short response time, and satisfactory LOD in the fg mL^{-1} range.

4. Conclusions

The present work reported the successful development of a novel disposable and affordable immunosensor made of inexpensive materials for the detection of SARS-CoV-2 spike protein (production cost = 0.29 USD per test unit). The electrochemical device was constructed using carbon ink-based SPE on PET substrate, which was modified with AuNPs-decorated CB dispersion. The immunosensor was applied for rapid POC diagnoses of SARS-CoV-2 spike protein and/or sensitive environmental analyses using calibration protocols based on two different incubation periods (10 min and 120 min). The application of the proposed immunosensor under the 120 min incubation regime resulted in higher sensitivity (~2.7 fold) compared to the 10 min incubation regime. The LOD values obtained from the successful application of the sensor for rapid diagnosis of SARS-CoV-2 in different samples under the 10 min and 120 min incubation regimes were 101 fg mL^{-1} and 46.2 fg mL^{-1} , respectively. The results obtained in this study show that the proposed biosensor can be effectively employed as a suitable tool for SARS-CoV-2 mass testing in low-income countries, and

can be easily adapted for different applications.

CRediT authorship contribution statement

Luís M.C. Ferreira: Conceptualization, Methodology, Data curation, Investigation, Writing – original draft, Writing – review & editing. **Isabela F. Reis:** Data curation, Investigation, Methodology. **Paulo R. Martins:** Formal analysis, Methodology. **Luiz H. Marcolino-Junior:** Conceptualization, Resources, Writing – review & editing. **Marcio F. Bergamini:** Conceptualization, Resources, Writing – review & editing. **Jessica R. Camargo:** Methodology. **Bruno C. Janegitz:** Conceptualization, Project administration, Resources, Funding acquisition, Writing – review & editing. **Fernando C. Vicentini:** Conceptualization, Resources, Funding acquisition, Supervision, Writing – review & editing.

Declaration of Competing Interest

The authors declare that they have no known competing financial interests or personal relationships that could have appeared to influence the work reported in this paper.

Data availability

Data will be made available on request.

Acknowledgments

The authors are extremely grateful to the Coordenação de Aperfeiçoamento de Pessoal de Nível Superior (CAPES) (financial code 001 and CAPES 09/2020 Epidemias 88887.644701/2021-00 and 88887.504861/2020-00), Conselho Nacional de Desenvolvimento Científico e Tecnológico (CNPq) (403961/2021-1; 311290/2020-5, 309803/2020-9, 402195/2020-5 and 408309/2018-0) and Fundação

Araucária (PBA2022011000056) for the financial assistance provided in support of this research. Representative schemes and graphical abstracts were prepared using BioRender as an auxiliary drawing tool.

Supplementary materials

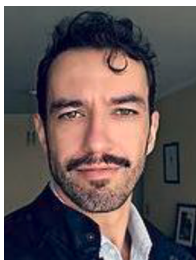
Supplementary material associated with this article can be found, in the online version, at [doi:10.1016/j.talo.2023.100201](https://doi.org/10.1016/j.talo.2023.100201).

References

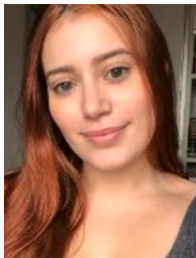
- [1] D.S. Hui, I.A. E, T.A. Madani, F. Ntoumi, R. Kock, O. Dar, G. Ippolito, T.D. McHugh, Z.A. Memish, C. Drosten, A. Zumla, E. Petersen, The continuing 2019-nCoV epidemic threat of novel coronaviruses to global health - The latest 2019 novel coronavirus outbreak in Wuhan, China, *Int. J. Infect. Dis.* 91 (2020) 264–266, <https://doi.org/10.1016/j.ijid.2020.01.009>.
- [2] P.G. Gottschalk, J.R. Dunn, The five-parameter logistic: a characterization and comparison with the four-parameter logistic, *Anal. Biochem.* 343 (1) (2005) 54–65, <https://doi.org/10.1016/j.ab.2005.04.035>.
- [3] A. Chaqroun, C. Hartard, E. Schvoerer, Anti-SARS-CoV-2 vaccines and monoclonal antibodies facing viral variants, *Viruses* 13 (6) (2021) 1171, <https://doi.org/10.3390/v13061171>.
- [4] I. Hadj Hassine, Covid-19 vaccines and variants of concern: a review, *Rev. Med. Virol.* (2021), <https://doi.org/10.1002/rmv.2313>.
- [5] T. Farooqi, J.A. Malik, A.H. Mulla, T. Al Hagbani, K. Almansour, M.A. Ubaid, S. Alghamdi, S. Anwar, An overview of SARS-CoV-2 epidemiology, mutant variants, vaccines, and management strategies, *J. Infect. Public Health* 14 (10) (2021) 1299–1312, <https://doi.org/10.1016/j.jiph.2021.08.014>.
- [6] N. Wiktorczyk-Kapischke, K. Grudlewska-Buda, E. Walecka-Zacharska, J. Kwiecińska-Pirog, L. Radtke, E. Gospodarek-Komkowska, K. Skowron, SARS-CoV-2 in the environment-Non-droplet spreading routes, *Sci. Total Environ.* 770 (2021), 145260, <https://doi.org/10.1016/j.scitotenv.2021.145260>.
- [7] I. Chakraborty, P. Maity, COVID-19 outbreak: migration, effects on society, global environment and prevention, *Sci. Total Environ.* 728 (2020), 138882, <https://doi.org/10.1016/j.scitotenv.2020.138882>.
- [8] A.B. Aziz, R. Raqib, W.A. Khan, M. Rahman, R. Haque, M. Alam, K. Zaman, A. G. Ross, Integrated control of COVID-19 in resource-poor countries, *Int. J. Infect. Dis.* 101 (2020) 98–101, <https://doi.org/10.1016/j.ijid.2020.09.009>.
- [9] A.L. Ferreira, L.F. de Lima, M.T. Torres, W.R. de Araujo, C. de la Fuente-Nunez, Low-cost optodiagnostic for minute-time scale detection of SARS-CoV-2, *ACS Nano* (2021), <https://doi.org/10.1021/acsnano.1c03236>.
- [10] B.D. Ventura, M. Cennamo, A. Minopoli, R. Campanile, S.B. Censi, D. Terracciano, G. Portella, R. Velotta, Colorimetric test for fast detection of SARS-CoV-2 in nasal and throat swabs, *ACS Sensors* 5 (10) (2020) 3043–3048, <https://doi.org/10.1021/acssensors.0c01742>.
- [11] B. Mojsoska, S. Larsen, D.A. Olsen, J.S. Madsen, I. Brandslund, F.A. Alatraktchi, Rapid SARS-CoV-2 detection using electrochemical immunosensor, *Sensors (Basel)* 21 (2) (2021), <https://doi.org/10.3390/s21020390>.
- [12] H. Zhao, F. Liu, W. Xie, T.C. Zhou, J. OuYang, L. Jin, H. Li, C.Y. Zhao, L. Zhang, J. Wei, Y.P. Zhang, C.P. Li, Ultrasensitive sandwich-type electrochemical sensor for SARS-CoV-2 from the infected COVID-19 patients using a smartphone, *Sens Actuators B Chem.* 327 (2021), 128899, <https://doi.org/10.1016/j.snb.2020.128899>.
- [13] M.S. Kumar, R. Nandeshwar, S.B. Lad, K. Megha, M. Mangat, A. Butterworth, C. W. Knapp, M. Knapp, P.A. Hoskisson, D.K. Corrigan, A.C. Ward, K. Kondabagil, S. Tallur, Electrochemical sensing of SARS-CoV-2 amplicons with PCB electrodes, *Sensors and Actuators B: Chem.* 343 (2021), 130169, <https://doi.org/10.1016/j.snb.2021.130169>.
- [14] L.F. de Lima, A.L. Ferreira, M.D.T. Torres, W.R. de Araujo, C. de la Fuente-Nunez, Minute-scale detection of SARS-CoV-2 using a low-cost biosensor composed of pencil graphite electrodes, *Proc. Natl. Acad. Sci. U. S. A.* 118 (30) (2021), <https://doi.org/10.1073/pnas.2106724118>.
- [15] V. Vasquez, M.C. Navas, J.A. Jaimes, J. Orozco, SARS-CoV-2 electrochemical immunosensor based on the spike-ACE2 complex, *Anal. Chim. Acta* 1205 (2022), 339718, <https://doi.org/10.1016/j.aca.2022.339718>.
- [16] D. Soto, J. Orozco, Peptide-based simple detection of SARS-CoV-2 with electrochemical readout, *Anal. Chim. Acta* 1205 (2022), 339739, <https://doi.org/10.1016/j.aca.2022.339739>.
- [17] A. Raziq, A. Kidakova, R. Boroznjak, J. Reut, A. Opik, V. Syrtiski, Development of a portable MIP-based electrochemical sensor for detection of SARS-CoV-2 antigen, *Biosens. Bioelectron.* 178 (2021), 113029, <https://doi.org/10.1016/j.bios.2021.113029>.
- [18] H.F. El Sharif, S.R. Dennison, M. Tully, S. Crossley, W. Mwangi, D. Bailey, S. P. Graham, S.M. Reddy, Evaluation of electropolymerized molecularly imprinted polymers (E-MIPs) on disposable electrodes for detection of SARS-CoV-2 in saliva, *Anal. Chim. Acta* 1206 (2022), 339777, <https://doi.org/10.1016/j.aca.2022.339777>.
- [19] S. Eissa, M. Zourob, Development of a low-cost cotton-tipped electrochemical immunosensor for the detection of SARS-CoV-2, *Anal. Chem.* 93 (3) (2021) 1826–1833, <https://doi.org/10.1021/acs.analchem.0c04719>.
- [20] L. Fabiani, M. Saroglia, G. Galata, R. De Santis, S. Fillo, V. Luca, G. Faggioni, N. D'Amore, E. Regalbutto, P. Salvatori, G. Terova, D. Moscone, F. Lista, F. Arduini, Magnetic beads combined with carbon black-based screen-printed electrodes for COVID-19: a reliable and miniaturized electrochemical immunosensor for SARS-CoV-2 detection in saliva, *Biosens. Bioelectron.* 171 (2021), 112686, <https://doi.org/10.1016/j.bios.2020.112686>.
- [21] G. Seo, G. Lee, M.J. Kim, S.H. Baek, M. Choi, K.B. Ku, C.S. Lee, S. Jun, D. Park, H. G. Kim, S.J. Kim, J.O. Lee, B.T. Kim, E.C. Park, S.I. Kim, Rapid detection of COVID-19 causative virus (SARS-CoV-2) in human nasopharyngeal swab specimens using field-effect transistor-based biosensor, *ACS Nano* 14 (4) (2020) 5135–5142, <https://doi.org/10.1021/acsnano.0c02823>.
- [22] D. Lu, D.Z. Zhu, H. Gan, Z. Yao, Q. Fu, X. Zhang, Prospects and challenges of using electrochemical immunosensors as an alternative detection method for SARS-CoV-2 wastewater-based epidemiology, *Sci. Total Environ.* 777 (2021), 146239, <https://doi.org/10.1016/j.scitotenv.2021.146239>.
- [23] I.-H. Cho, D.H. Kim, S. Park, Electrochemical biosensors: perspective on functional nanomaterials for on-site analysis, *Biomater. Res.* 24 (1) (2020), <https://doi.org/10.1186/s40824-019-0181-y>.
- [24] F. Arduini, S. Cinti, V. Mazzaracchio, V. Scognamiglio, A. Amine, D. Moscone, Carbon black as an outstanding and affordable nanomaterial for electrochemical (bio)sensor design, *Biosens. Bioelectron.* 156 (2020), 112033, <https://doi.org/10.1016/j.bios.2020.112033>.
- [25] L.C. Brazaca, A.H. Imamura, N.O. Gomes, M.B. Almeida, D.T. Scheidt, P. A. Raymundo-Pereira, O.N. Oliveira Jr., B.C. Janegitz, S.A.S. Machado, E. Carrilho, Electrochemical immunosensors using electrodeposited gold nanostructures for detecting the S proteins from SARS-CoV and SARS-CoV-2, *Anal. Bioanal. Chem.* (2022), <https://doi.org/10.1007/s00216-022-03956-1>.
- [26] S. Alim, J. Vejayan, M.M. Yusoff, A.K.M. Kafi, Recent uses of carbon nanotubes & gold nanoparticles in electrochemistry with application in biosensing: a review, *Biosens. Bioelectron.* 121 (2018) 125–136, <https://doi.org/10.1016/j.bios.2018.08.051>.
- [27] I. Khalil, N. Julkapli, W. Yehye, W. Basirun, S. Bhargava, Graphene-gold nanoparticles hybrid—synthesis, functionalization, and application in a electrochemical and surface-enhanced Raman scattering biosensor, *Materials (Basel)* 9 (6) (2016) 406, <https://doi.org/10.3390/ma9060406>.
- [28] K.R. Brown, D.G. Walter, M.J. Natan, Seeding of colloidal Au nanoparticle solutions. 2. Improved control of particle size and shape, *Chem. Mater.* 12 (2000) 306–313.
- [29] R.C. Freitas, L.O. Orzari, L.M.C. Ferreira, T.R.L.C. Paixão, W.K.T. Coltro, F. C. Vicentini, B.C. Janegitz, Electrochemical determination of melatonin using disposable self-adhesive inked paper electrode, *J. Electroanal. Chem.* 897 (2021), <https://doi.org/10.1016/j.jelechem.2021.115550>.
- [30] J.R. Camargo, I.A. Andreotti, C. Kalinke, J.M. Henrique, J.A. Bonacin, B. C. Janegitz, Waterproof paper as a new substrate to construct a disposable sensor for the electrochemical determination of paracetamol and melatonin, *Talanta* 208 (2020), 120458, <https://doi.org/10.1016/j.talanta.2019.120458>.
- [31] I.A. de Araujo Andreotti, L.O. Orzari, J.R. Camargo, R.C. Faria, L.H. Marcolino-Junior, M.F. Bergamini, A. Gatti, B.C. Janegitz, Disposable and flexible electrochemical sensor made by recyclable material and low cost conductive ink, *J. Electroanal. Chem.* 840 (2019) 109–116, <https://doi.org/10.1016/j.jelechem.2019.03.059>.
- [32] M. Björklund, A.C. Ouweland, S.D. Forssten, Improved artificial saliva for studying the cariogenic effect of carbohydrates, *Curr. Microbiol.* 63 (1) (2011) 46–49, <https://doi.org/10.1007/s00284-011-9937-x>.
- [33] C.A. Holstein, M. Griffin, J. Hong, P.D. Sampson, Statistical method for determining and comparing limits of detection of bioassays, *Anal. Chem.* 87 (19) (2015) 9795–9801, <https://doi.org/10.1021/acs.analchem.5b02082>.
- [34] C. Jeyabharathi, P. Ahrens, U. Hasse, F. Scholz, Identification of low-index crystal planes of polycrystalline gold on the basis of electrochemical oxide layer formation, *J. Solid State Electrochem.* 20 (11) (2016) 3025–3031, <https://doi.org/10.1007/s10008-016-3228-1>.
- [35] A. Sukeri, M. Bertotti, Nanoporous gold surface: an efficient platform for hydrogen evolution reaction at very low overpotential, *J. Braz. Chem. Soc.* (2017), <https://doi.org/10.21577/0103-5053.20170132>.
- [36] A.P. O'Mullane, From single crystal surfaces to single atoms: investigating active sites in electrocatalysis, *Nanoscale* 6 (8) (2014) 4012–4026, <https://doi.org/10.1039/c4nr00419a>.
- [37] B. Jin, Jim-Rong, Z.-X. Zhang, Theory and application of cyclic voltammetry for measurement of fast electrode kinetics at microdisk electrode, *Chin. J. Chem.* 14 (4) (1996) 338–347.
- [38] S.A. Perdomo, V. Ortega, A. Jaramillo-Botero, N. Mancilla, J.H. Mosquera-DeLaCruz, D.P. Valencia, M. Quimbaya, J.D. Contreras, G.E. Velez, O.A. Loaiza, A. Gomez, J. de la Roche, SenSARS: a low-cost portable electrochemical system for ultra-sensitive, near real-time, diagnostics of SARS-CoV-2 infections, *IEEE Trans. Instrum. Meas.* 70 (2021) 1–10, <https://doi.org/10.1109/tim.2021.3119147>.
- [39] J. Munoz, M. Pumera, 3D-printed COVID-19 immunosensors with electronic readout, *Chem. Eng. J.* 425 (2021), 131433, <https://doi.org/10.1016/j.cej.2021.131433>.
- [40] M.D.T. Torres, W.R. de Araujo, L.F. de Lima, A.L. Ferreira, C. de la Fuente-Nunez, Low-cost biosensor for rapid detection of SARS-CoV-2 at the point of care, *Matter* 4 (7) (2021) 2403–2416, <https://doi.org/10.1016/j.matt.2021.05.003>.
- [41] P. Lasserre, B. Balanethupathy, V.J. Vezza, A. Butterworth, A. Macdonald, E. O. Blair, L. McAteer, S. Hannah, A.C. Ward, P.A. Hoskisson, A. Longmuir, S. Setford, E.C.W. Farmer, M.E. Murphy, H. Flynn, D.K. Corrigan, SARS-CoV-2 aptasensors based on electrochemical impedance spectroscopy and low-cost gold

electrode substrates, Anal. Chem. (2022), <https://doi.org/10.1021/acs.analchem.1c04456>.

- [42] N.K. Singh, P. Ray, A.F. Carlin, C. Magallanes, S.C. Morgan, L.C. Laurent, E. S. Aronoff-Spencer, D.A. Hall, Hitting the diagnostic sweet spot: point-of-care SARS-CoV-2 salivary antigen testing with an off-the-shelf glucometer, Biosens. Bioelectron. 180 (2021), 113111, <https://doi.org/10.1016/j.bios.2021.113111>.
- [43] D. Liu, C. Ju, C. Han, R. Shi, X. Chen, D. Duan, J. Yan, X. Yan, Nanozyme chemiluminescence paper test for rapid and sensitive detection of SARS-CoV-2 antigen, Biosens. Bioelectron. 173 (2020), 112817, <https://doi.org/10.1016/j.bios.2020.112817>.



Luís M. C. Ferreira graduated in chemistry (Universidade Federal de Juiz de Fora) in 2008, moved to USP-São Paulo where concluded his master (2011) and Ph.D. (2016) with emphasis in analytical chemistry. Started as post-doctoral researcher at Universidade Federal de São Carlos in 2020. Luís has experience in the construction of electrochemical sensors and biosensors based on screen-printed electrodes modified with nanobiomaterials and metalloporphyrins.



Isabela F. Reis Undergraduate environmental engineering student at Universidade Federal de São Carlos since 2018. Works under supervision of prof. Fernando Campanhã Vicentini on the research of electrochemical biosensors toward environmental analysis.



Paulo R. Martins Graduated in chemistry (Universidade Federal de Santa Maria) in 2007 and concluded his Ph.D. in inorganic chemistry at USP-São Paulo, where finished his and postdoctoral research. Started to teach at Universidade Federal de Goiás at 2014 and works on research based on electrochemistry and development on new materials for energy storage devices and sensors.

Luiz H. Marcolino-Junior received his Ph.D. in Chemistry from Universidade Federal de São Carlos (UFSCar), Brazil, in 2007. He is a professor in the Chemistry Department at Universidade Federal do Paraná (DQ-UFPR). His-current research interests are the development of electrochemical sensors using nanostructured materials and the development of microfluidic devices with electrochemical response.



Marcio F. Bergamini received his Ph.D. in Analytical Chemistry in 2007 from Universidade Estadual Paulista (UNESP), Araraquara-SP, Brazil. He is currently a Professor of Chemistry at the Federal University of Paraná (UFPR), Curitiba-PR, Brazil. His-principal research interest comprises the development of a new electrochemical sensor for the determination of inorganic and organic compounds in pharmaceutical, biological, or environmental samples.



Jessica R. Camargo graduated in chemistry at Universidade Federal de São Carlos in 2019 and started her Ph.D. at the same institution in 2020. She works on research in materials science and electrochemistry focused development of sensors and biosensors.



Bruno Campos Janegitz received Ph.D. degree from Federal University of São Carlos, in 2012. He was a postdoctoral researcher at University of São Paulo between 2012 and 2014. At present, he is Professor at Federal University of São Carlos. His-research interests include electroanalytical chemistry, nanostructured electrode materials and modified electrode surfaces, electrochemical sensors and biosensors for medical and environmental analysis.



Fernando Campanhã Vicentini received his MS degree in Chemistry from the University of São Paulo, São Carlos, SP (Brazil) in 2009 and PhD degree in Analytical chemistry from the Federal University of São Carlos, São Carlos, SP (Brazil) in 2013. He was a postdoctoral researcher at Federal University of São Carlos between 2013 and 2015. Currently, he is associate professor at Federal University of São Carlos, Buri, SP (Brazil). His-research interests include the study of new electrode materials, CNTs, graphene, carbon black, carbon materials, metallic and metal oxide nanoparticles, hybrid materials, polymers, ultrathin films, nanostructured materials and the development of electrochemical sensors and biosensors for environmental, medical and clinical samples.